UC Irvine
UC Irvine Previously Published Works

Title

New particle formation and growth in an isoprene-dominated ozark forest: From sub-5 nm to CCN-active sizes

Permalink

https://escholarship.org/uc/item/0vj4p0hw

Journal

Aerosol Science and Technology, 48(12)

ISSN

0278-6826

Authors

Yu, H
Ortega, J
Smith, JN
et al.

Publication Date

2014-12-02

DOI

10.1080/02786826.2014.984801

Copyright Information

Peer reviewed

New Particle Formation and Growth in an Isoprene-Dominated Ozark Forest: From Sub-5 nm to CCN-Active Sizes

Huan Yu,[1,2] John Ortega,[3] James N. Smith,[3,4] Alex B. Guenther,[5,6] V. P. Kanawade,[7] Yi You,[2] Yiying Liu,[2,8] Kevin Hosman,[9] Thomas Karl,[10] Roger Seco,[3,11] Chris Geron,[12] Stephen G. Pallardy,[9] Lianhong Gu,[13] Jyri Mikkilä,[14] and Shan-Hu Lee[2]

[1]*School of Environmental Science and Engineering, Nanjing University of Information Science and Technology, Nanjing, China*
[2]*College of Public Health, Kent State University, Kent, Ohio, USA*
[3]*Atmospheric Chemistry Division, National Center for Atmospheric Research, Boulder, Colorado, USA*
[4]*Applied Physics Department, University of Eastern Finland, Kuopio, Finland*
[5]*Department of Civil and Environmental Engineering, Washington State University, Pullman, Washington, USA*
[6]*Pacific Northwest National Laboratory, Richland, Washington, USA*
[7]*Department of Civil Engineering and Center for Environmental Science and Engineering, Indian Institute of Technology, Kanpur, India*
[8]*Epidemiology and Biostatistics Department, Case Western Reserve University, Cleveland, Ohio, USA*
[9]*Department of Forestry, University of Missouri, Columbia, Montana, USA*
[10]*Institute for Meteorology and Geophysics, University of Innsbruck, Innsbruck, Austria*
[11]*Department of Earth System Science, University of California, Irvine, California, USA*
[12]*Office of Research and Development, U.S. Environmental Protection Agency, Durham, North Carolina, USA*
[13]*Oak Ridge National Laboratory, Environmental Sciences Division, Oak Ridge, Tennessee, USA*
[14]*AirModus, Helsinki, Finland*

Particle Investigations at a Northern Ozarks Tower: NOx, Oxidant, Isoprene Research (PINOT NOIR) were conducted in a Missouri forest dominated by isoprene emissions from May to October 2012. This study presents results of new particle formation (NPF) and the growth of new particles to cloud condensation nuclei (CCN)-active sizes ($\sim$100 nm) observed during this field campaign. The measured sub-5 nm particles were up to $\sim$20,000 cm^{-3} during a typical NPF event. Nucleation rates J_1 were relatively high (11.0 $\pm$ 10.6 cm^{-3} s^{-1}), and one order of magnitude higher than formation rates of 5 nm particles (J_5). Sub-5 nm particle formation events were observed during 64% of measurement days, with a high preference in biogenic volatile organic compounds (BVOCs)- and SO$_2$-poor northwesterly (90%) air masses than in BVOCs-rich southerly air masses (13%). About 80% of sub-5 nm particle events led to the further growth. While high temperatures and high aerosol loadings in the southerly air masses were not favorable for nucleation, high BVOCs in the southerly air masses facilitated the growth of new particles to CCN-active sizes. In overall, 0.4–9.4% of the sub-5 nm particles grew to CCN-active sizes within each single NPF event. During a regional NPF event period that took place consecutively over several days, concentrations of CCN size particles increased by a factor of 4.7 in average. This enhanced production of CCN particles from new particles was commonly observed during all 13 regional NPF events during the campaign period.

---

1. INTRODUCTION

New particle formation (NPF) can account for a significant production of global cloud condensation nuclei (CCN). Global and regional model simulations have shown newly formed particles can contribute to 3–70% of the global CCN production (Spracklen et al. 2008; Pierce and Adams 2009;

Yu and Luo 2009; Matsui et al. 2013). The large uncertainties in modeling estimations are due to uncertainties in aerosol nucleation and growth rates, as well as primary aerosol emissions. Field studies conducted in urban and suburban (Laaksonen et al. 2005; Wiedensohler et al. 2009; Yue et al. 2011; Wang et al. 2013) and pristine sites (Lihavainen et al. 2003; Kerminen et al. 2005) have shown that NPF can indeed enhance local CCN concentrations by a factor of 1.9–7.0. Field observations are needed, as they can be used to evaluate model predictions, but such observations are still scarce.

Forests are a major source of biogenic volatile organic compounds (BVOCs) in the atmosphere (Guenther et al. 1995) and thus serve as an important source of secondary aerosol particles. NPF has been observed in various forest environments, such as the Finland boreal forest (Mäkelä et al. 1997; Sihto et al. 2006), European coniferous forests (Held et al. 2004) and African savanna forests (Laakso et al. 2008). Bonn and colleagues have suggested that oxidation products of monoterpenes (MT) and sesquiterpenes, together with sulfuric acid (H_2SO_4), are likely precursors of new particles in boreal forest environments (Bonn and Moortgat 2002, 2003; Bonn et al. 2007, 2008, 2009). Measurements made in the Hyytiälä boreal forest have shown that sub-3 nm particles were, in general, positively correlated with the first generation products of MT ozonolysis reactions (Ehn et al. 2010; Lehtipalo et al. 2011; Ortega et al. 2012; Riccobono et al. 2012; Kulmala et al. 2013). Ehn et al. (2014) recently showed that a group of extremely low-volatility highly-oxidized organic compounds, formed from the photo-oxidation and ozonolysis of α-pinene, can explain the measured growth of sub-5 nm particles in Hyytiälä. The importance of MT on NPF has also been verified by laboratory experiments (Zhang et al. 2009; Schobesberger et al. 2013; Zhao et al. 2013).

Isoprene, emitted from broad leaf trees, is the most abundant BVOC species at the global scale (Guenther et al. 1995). But it is unclear how isoprene participates in the biogenic NPF and growth processes in forest environments. Kiendler-Scharr and colleagues have suggested, from their plant chamber experiments, that isoprene likely suppresses NPF when isoprene-to-MT ratios exceed a certain threshold (e.g., >1) (Kiendler-Scharr et al. 2009; Kiendler-Scharr et al. 2012). Consistent with their laboratory studies, field measurements in a mixed deciduous forest in Michigan showed rare NPF occurrences, under high isoprene-to-MT ratio conditions (Kanawade et al. 2011). A large number of observations were made in Amazon rainforests with high emissions of isoprene, and these studies have also consistently showed an absence of NPF (Poschl et al. 2010; Pöhlker et al. 2012). Contrary to such hypothesis on the possible suppression of NPF, Surratt and colleagues suggested that oxidation products of isoprene (e.g., IEPOX) can actually promote the growth of new particles (Surratt et al. 2010; Lin et al. 2013).

To understand the effect of BVOCs on the formation of new particles and their subsequent growth to CCN in real forest environments, we have conducted aerosol size distribution and volatile organic compounds (VOCs) measurements in a Missouri forest during the Particle Investigations at a Northern Ozarks Tower: NO_x, Oxidant, Isoprene Research (PINOT NOIR) field campaign from May to October 2012. The campaign site was located in the ecologically important transitional zone between the hardwood and grassland regions of the central U.S. In the present study, we have investigated survival rates of new particles to CCN-active size particles (~100 nm), and the enhancement of CCN particles during regional NPF events.

2. MEASUREMENTS

The Ozarks forest site (38.74 °N, 92.20 °W) is located to the north of the Ozark Plateau in the Central United States. The canopy height ranges from 17–25 m with a leaf area index of 4.2 m^2 m^{-2}. This forest is predominantly composed of oak (*Quercus velutina, Q. alba,* and *Q. rubra*) and hickory trees (*Carya* spp.), and this region is referred as a so-called "isoprene volcano" zone (Wiedinmyer et al. 2005; Potosnak et al. 2014). The isoprene-to-MT carbon ratio was 15.3 ± 7.2 during the campaign period. This ratio was close to those found in Amazonian rain forests (e.g., 15.2; Greenberg et al. 2004) where NPF was not observed at the ground level, but much higher than 0.18 observed in the Finland boreal forest (Spirig et al. 2004) where frequent NPF was observed.

Instruments deployed during the campaign are listed in Table 1. Particle measurements were conducted in an air-conditioned shed, with sampling inlets located at ~3.7 m above the ground. As our sampling site was located on the edge of a small clearing, we expect there to be a greater degree of coupling with the above canopy air than would otherwise be the case for the below canopy environment and so our measurements represent something in between the below-canopy and above-canopy environments. We did have simultaneous above canopy measurements with a PTRMS at the site which indicated that isoprene and monoterpenes concentrations at this surface sampling location were similar to the levels observed in the above canopy environment.

Ambient air was sampled to a scanning mobility particle spectrometer, SMPS (TSI 3085 differential mobility analyzer, DMA, coupled with a TSI 3776 condensation particle counter, CPC) and an optical particle counter (OPC) via a 4.8 mm inner diameter copper tube, erected vertically outside the shed (total length: 7.3 m). The total flow rate through the inlet tubing was 2 standard liters per minute (slpm), which was split equally between the SMPS and OPC. The OPC was modified from a commercially available passive cavity aerosol spectrometer probe (PCASP, Droplet Measurement Technologies) which detects single particles from 50 nm to ~2 μm by light

TABLE 1
Summary of instruments deployed in the Northern Ozarks site, Missouri, during May–October 2012 for the PINOT NOIR
campaign. NH_3 concentrations were predicted from the MOZART-4/GEOS5 model

Instrument	Species measured	Time resolution
Entire campaign: 4 May–20 October 2012		
Nano-SMPS (TSI 3085 and CPC 3776)	Particle size distribution in the size range from 5–115 nm	5 min
OPC (DMT, PCASP)	Particle size distribution in the size range from 110–3000 nm	5 min
PTR-QMS (Ionicon Analytik GmbH)	VOCs	30 min
Meteorological sensors	Temperature, RH, shortwave radiation, precipitation, wind speed, and direction	30 min
UV absorption O_3 analyzer (Teledyne Technologies Incorporated, 400E)	O_3	24 h
MOZART-4/GEOS-5	NH_3	6 h
Intensive observation period: 1 August–18 October 2012		
PSM (Airmodus A09)	Total number concentration of >1 nm particles	1 s
SO_2 analyzer (Thermo Scientific, Model 43i)	SO_2	24 h
Supplementary measurements: 28 July–8 August 2012		
PTR-TOF-MS (Ionicon Analytik GmbH)	VOCs	1 min

scattering within an optical cavity using a He:Ne laser (632.8 nm wavelength). We tested the OPC with PSL spheres to ensure that the particle diameters from 100–1000 nm were accurately reflected in the OPC data. It has been tested in the laboratory that the raw OPC values were ∼5 times lower than the SMPS values in the overlapped size range (∼50–150 nm), but agreed well in the larger sizes. So, we scaled down the total number counts from the OPC starting from 110 nm to 150 nm with a factor of 5 to match the counts at the 110 nm channel from the nano-SMPS. By doing this, smooth size distributions were obtained in the size range of 50–150 nm for the majority of the campaign (May–October 2012). Total number concentrations of particles in the size range from 5–3000 nm ($N_{SMPS+OPC}$) were obtained by integrating the SMPS (5–110 nm) and OPC (110–3000 nm) measurements. Particle losses in the size range below 30 nm were corrected by taking into account particle transport efficiencies in the sampling inlet, using a particle loss calculator tool developed by von der Weiden et al. (2009). Number concentrations of particles in the size range of 5–25 nm (N_{5-25}) were calculated from the SMPS measurements. Number concentrations of particles in the size range from 100–500 nm ($N_{100-500}$) were derived by integrating SMPS (100–110 nm) and OPC measurements (110–500 nm). Typically, ∼100 nm has been assumed as the CCN-active diameter for soluble particles at 0.2% super saturation in the literature (Kuang et al. 2009; Pierce and Adams 2009). From our size distribution measurements, we found that 500 nm particles contributed to only ∼0.07% of N_{100} and also new particles seldom grew larger than 500 nm after NPF

events at this site. Thus, we used $N_{100-500}$ as the surrogate of CCN-active particles. It is possible that the actual CCN concentrations may be different from $N_{100-500}$ concentrations, but this was considered as the best measure of the potential of CCN productions without CCN measurements at the site.

Total number concentrations of particles down to 1 nm diameter (N_{PSM}) were measured with a particle size magnifier (PSM, AirModus A09) using diethylene glycol (DEG) as the working fluid at a fluid flow rate of 1 standard litter per minute (slpm) (Vanhanen et al. 2011). A PSM can grow particles as small as 1 nm to larger than 90 nm, after which a CPC is used to count the grown particles. The PSM sampled the ambient air via a 37-cm long and 4.8-mm inner diameter copper tube, at a flow rate of 90 slpm. The PSM was then connected to the copper tube, further through a flexible 5-cm long and 4.1-mm inner diameter conductive silica tube. The number concentrations of 5–3000 nm particles counted by the PSM ($N'_{SMPS+OPC}$) were derived from the measured $N_{SMPS+OPC}$ and particle loss rates in the copper and silica tubes. The differences between N_{PSM} and $N'_{SMPS+OPC}$ correspond to sub-5 nm particle number concentrations counted by the PSM. The transport loss of sub-5 nm particles in the PSM inlet, estimated with a particle loss calculator tool developed by others (von der Weiden et al. 2009), was 10% and 39% for 5 nm to 1.3 nm particles, respectively. Because the exact size distribution in the 1–5 nm size range were unknown from PSM measurements, sub-5 particle number concentrations (N_{sub-5}) were corrected using an "average" transport loss of 18% at 2.5 nm particles. Depending on actual particle sizes (within 1–5 nm),

the $N_{\text{sub-5}}$ derived from an average transport loss rate of 18% were between 74.4% and 109.8% of the actual sub-5 nm particle number concentrations present in the atmosphere. Therefore, the uncertainty in $N_{\text{sub-5}}$ due to particle loss correction was estimated to be up to 25%. The SMPS and OPC were operated during the entire campaign (4 May to 21 October 2012), and the PSM was only during the intensive observation period (IOP; 1 August to 18 October 2012).

A proton transfer reaction quadrupole mass spectrometer (PTR-QMS, Ionicon) and meteorological sensors were deployed on an instrumented tower, 30 m above the ground level and 8 m above the canopy. The PTR-QMS measured key BVOCs, including isoprene (ion mass to charge ratio m/z 69), methylvinylketone and methacrolein isomers (m/z 71), MT isomers (m/z 137), and hydroxyacetone (m/z 75). Detection limit of the PTR-QMS is 1 pptv with an integration time of 1 min. Between 28 July and 8 August, a proton transfer reaction time-of-flight mass spectrometer (PTR-ToF-MS, Ionicon) was also deployed at the ground level. Detection limits with PTR-ToF-MS are in the range of 1–20 pptv depending on compounds and the accuracy is ±15% (Kaser et al. 2013).

Sulfur dioxide (SO_2) and ozone (O_3) data were obtained from an U.S. Environmental Protection Agency (EPA) monitoring station in the Mark Twain State Park. The station is about 30 km to the north of the Ozarks Tower (http://www.epa.gov/airdata/ad_maps.html), and monitors the regional background SO_2 and O_3 mixing ratios in the area. Detection limit of SO_2 analyzer (Thermo Scientific, Model 43i) is 0.058–0.095 ppbv with an uncertaint+y of ±10%. Detection limit of UV absorption O_3 analyzer (Teledyne Technologies Incorporated, 400E) is 0.6 ppbv with an uncertainty of ±5%. NH_3 was not measured during the campaign, and we instead estimated 6-h average estimates of NH_3 mixing ratios between 4 May –21 October, from simulations conducted with the Model for Ozone and Related chemical Tracers Version 4 (MOZART-4) driven by NASA/GMAO/GEOS-5 meteorological fields (MOZART-4/GEOS-5). MOZART-4 utilized NH_3 emission inventories including anthropogenic sources, fires, soil, and ocean sources and the model evaluation was presented in Emmons et al. (2010).

Three-day backward trajectories were calculated from the NOAA Hybrid Single-Particle Lagrangian Integrated Trajectory (HYSPLIT) model (Draxler and Rolph 2003) at a height of 500 m hourly for each day during the entire campaign, in order to track the history of air masses within the mixing layer. Air masses, based on the back trajectory analysis, were identified into four different types of air mass: southerly (BVOC-rich air parcels passing over the Ozark forest), northeasterly (SO_2-rich), northwesterly (BVOC and SO_2-poor), and slow moving local air masses. Air masses that spent over 72 h within 200 km around the sampling site were referred to as slow moving local air masses.

3. PARTICLE FORMATION EVENT CHARACTERIZATION

In the present work, the sub-5 nm particle event was defined when a concentration ($N_{\text{sub-5}}$) greater than 2000 cm^{-3} persisted for longer than 3 h. An NPF event was defined, when sub-5 nm particles underwent a continuous growth for a few hours, as indicated by a typical particle growth curve in the measured aerosol size spectra. Based on Dal Maso et al. (2005), NPF events were further classified into two classes. In a Class-I NPF, particle size distributions displayed a daytime "banana-shaped" contour plot of a consecutive size growth. This is a conventional NPF event, from which new particle growth rate (GR), formation rate of 5 nm particles (J_5), and nucleation rate (J_1) were obtained. In a Class-II NPF event, there was a rather "broken" shaped contour in the size distribution, due to inhomogeneous mixing of air masses.

The condensation sink CS is a measure of how rapidly H_2SO_4 molecules condense onto pre-existing aerosols, based on (Kulmala et al. 2001):

$$CS = 2\pi D_j \sum_j \beta_{m,j} d_j N_j \qquad [1]$$

where

$$\beta_{m,j} = \frac{1 + Kn_j}{1 + 0.337 Kn_j + \frac{4Kn_j}{3\alpha} + \frac{4Kn_j}{3\alpha}} \qquad [2]$$

and

$$Kn_j = \frac{2\lambda_\upsilon}{d_j} \qquad [3]$$

$\beta_{m,j}$ is the size-dependent transition correction factor, Kn_j the Knudsen number, D the diffusion coefficient for H_2SO_4 (0.104 cm^2 s^{-1}), α mass accommodation coefficient (taken as the unity for H_2SO_4), and $\lambda\upsilon$ is the mean free path of the H_2SO_4 molecule (6.7 × 10^{-6} cm) at 1 atm and 298 K.

GR was determined by fitting the first order polynomial fit to the particle mode diameter in the size range from 5–25 nm (D_p) based on Dal Maso et al. (2005):

$$GR = \frac{dD_p}{dt} \qquad [4]$$

Particle formation rates were empirically determined from a simplified approximation of the general dynamic equation (GDE) (Seinfeld and Pandis 2006). Formation rate of 1 nm and 5 nm particles (J_1 and J_5) were calculated by taking into account coagulation losses and particle fluxes out of the

measured size ranges (Dal Maso et al. 2005):

$$J_5 = \frac{dN_{5-25}}{dt} + CoagS_{5-25} \times N_{5-25} + Gr\left(\frac{dN}{dD_p}\right)_{25nm} \quad [5]$$

$$J_1 = \frac{dN_{sub-5}}{dt} + CoagS_{sub-5} \times N_{sub-5} + J_5 \quad [6]$$

where dN/dt was determined by a linear fit between N and t. Coagulation sinks of 5–25 nm particles ($CoagS_{5-25}$) and sub-5 nm particles ($CoagS_{sub-5}$) were approximated, for a simplification, by those of 11 nm (geometric mean of 5 nm and 25 nm) and 2.5 nm (geometric mean of 1.3 nm and 5 nm) particles, respectively. Coagulation sink is expressed as $\sum_j K_{ij} N_j$, where N_j is the particle number concentration in size bin j, and K_{ij} is the coagulation coefficient between size bin j and the reference size i (i.e., in this case, 11 nm and 2.5 nm).

$$K_{ij} = 2\pi\left(d_i + d_j\right)\left(D_i + D_j\right)\beta_{F_{i,j}} \quad [7]$$

where d is the diameter of a size bin, D the size dependent diffusion coefficient, and β_F the Fuchs correction factor of particles.

4. RESULTS AND DISCUSSION

4.1. Sub-5 nm Particles and NPF Event Occurrences

During the total 170 measurement days from May to October, there were 37 Class-I NPF events and 38 Class-II NPF events (Table 1). NPF (Class-I and Class-II) was less frequent in the summer (33% in June and 23% in July) than in the spring and fall (about 50–60% in May, August, September, and October) (Table 2). This seasonal trend was consistent with those found in other locations, globally (Kulmala et al. 2004b; Zhang et al. 2012). NPF occurred during 85% of the days associated with clean northwesterly air masses, in contrast to only 9% of the days with BVOCs-rich southerly air masses. In northeasterly and local air masses, NPF frequency was 46% and 30%, respectively.

Sub-5 nm particle events took place with the same air masses preferable for NPF. During the 75 observation days between August and October, there were 48 events of sub-5 nm particles, all of which occurred during the daytime. Sub-5 nm particle events were observed on 90% of the days with northwesterly air masses, but only on 13% of the days with southerly air masses. In northeasterly and local air masses, the frequency was around 60%. The sub-5 nm particle event frequencies were 59%, 63%, and 72% in August, September, and October, respectively.

N_{sub-5} and N_{5-25} showed different diurnal variations (Figure 1). In the early morning, N_{sub-5} was around 1000 cm^{-3}, regardless of whether there was a sub-5 nm particle event or not. During non-event days, N_{sub-5} remained quite constant during the whole day. Also, N_{5-25} was quite constant ($\sim$80 cm^{-3}), one order of magnitude lower than N_{sub-5}. However, during the event days, N_{sub-5} increased by a factor of $\sim$20, reaching a maximum of $\sim$20,000 cm^{-3} around 11:30 AM local time, and then decreased slowly until the following morning. N_{5-25} also raised from $\sim$200 cm^{-3} in the early morning to $\sim$2500 cm^{-3} around 13:00 PM. There was a time delay of $\sim$1.5 h between N_{sub-5} peak and N_{5-25} peak, in which particle growth took place from the cluster mode to the nucleation mode.

The N_{sub-5} at the Northern Ozarks site was one order of magnitude higher, compared to N_{sub-3} measured at a semi-rural continental (Kent, OH, USA) and a coastal site (Brookhaven, NY, USA) (background level $\sim$200 cm^{-3}; peak level

TABLE 2
Summary of NPF and sub-5 nm particle formation events during the PINOT NOIR campaign. Both the number of events (total valid observation days) and the event frequency are shown here

| | | Sub-5 nm particle event | | NPF event | | | | | |
				Class-I		Class-II		Total	
Air mass type	S	2(15)	13.3%	1(56)	1.8%	4(56)	7.1%	5(56)	8.9%
	L	9(14)	64.3%	2(20)	10.0%	4(20)	20.0%	5(20)	30.0%
	NE	9(15)	60%	13(41)	31.7%	6(41)	14.6%	19(41)	46.3%
	NW	28(31)	90.3%	21(53)	39.6%	24(53)	45.3%	45(53)	84.9%
Month	May			6(28)	21.4%	11(28)	39.3%	17(28)	60.7%
	June			6(30)	20.0%	4(30)	13.3%	10(30)	33.3%
	July			5(31)	16.1%	2(31)	6.5%	7(31)	22.6%
	August	16(27)	59.2%	6(31)	19.4%	10(31)	32.3%	16(31)	51.6%
	September	19(30)	63.3%	8(30)	26.7%	7(30)	23.3%	15(30)	50.0%
	October	13(18)	72.2%	6(20)	30.0%	4(20)	20.0%	10(20)	50.0%
Mean		48(75)	64%	37(170)	21.8%	38(170)	22.4%	75(170)	44.1%

(a)

(b)

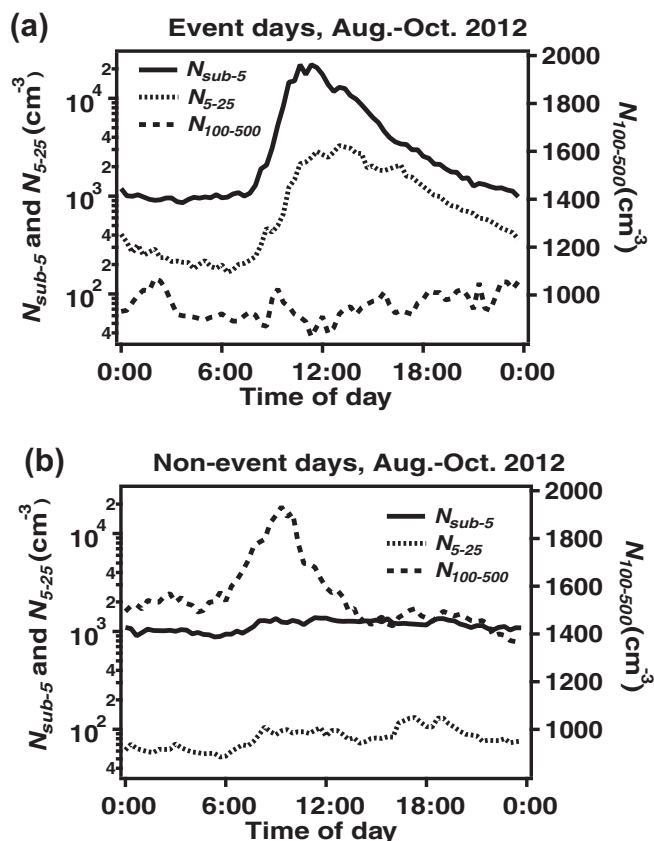FIG. 1. The diurnal variation of N_{sub-5}, N_{5-25}, and $N_{100-500}$ for the days without (upper panel) or with sub-5 nm particle formation events (lower panel). The lines represent the median of 20-min mean concentrations.

2000–3000 cm^{-3}) (Yu et al. 2014). The N_{sub-5} at this forest site was roughly on the same order of magnitude as sub-2 nm particle number concentrations (N_{sub-2}) reported from the Hyytiälä boreal forest, which varied between the background level of 2×10^3 cm^{-3} and the noontime peak of 9×10^3 cm^{-3} (Kulmala et al. 2013).

During NPF event periods, J_1 ranged from 0.8–42.6 cm^{-3} s^{-1} (Table 3). These J_1 values were compared with nucleation rates reported previously from other locations derived with different methods, as the following. For example, our J_1 values were similar to J_1 (0.1–40 cm^{-3} s^{-1}) measured in the boreal forest with a scanning PSM (Kulmala et al. 2013), but were much higher than those measured in Ohio and New York states with PSM (1.1–1.3 cm^{-3} s^{-1}; Yu et al. 2014). Our J_1 values were lower than those derived from SMPS measurements derived with the PARGAN model in a downwind site in Taiwan (40–113 cm^{-3} s^{-1}; Young et al. 2013), and were lower than J_1 extrapolated from J_3 measurements in Tecamac, Mexico (up to 10^4 cm^{-3} s^{-1}; Kuang et al. 2008) or in the boreal forest (0.1–1000 cm^{-3} s^{-1}; Kuang et al. 2008; Sihto et al. 2006). For the non-NPF event periods, we also calculated the background J_1, by ignoring the last term on the right hand side

of Equation (6). The background J_1 during non-event days was 0.1 ± 0.3 cm^{-3} s^{-1}. In comparison, at Ohio and New York, the background J_1 during the night was 0.13 cm^{-3} s^{-1} and 0.23 cm^{-3} s^{-1}, respectively (Yu et al. 2014). During non-event days in the boreal forest, the formation rate of 1.5 nm neutral clusters ranged from 0.1–0.4 cm^{-3} s^{-1} (Kulmala et al. 2013). Thus, background particle nucleation rates are fairly similar at these different sites.

Compared to J_1, J_5 were one order of magnitude lower (1.0 ± 1.1 cm^{-3} s^{-1}), implying that the majority of 1 nm new particles was lost by coagulation instead of growing from 1 nm to 5 nm. This also explains why not all sub-5 nm particles were developed into NPF events, as discussed above. The GR in the particle size range of 5–25 nm at the Ozark site were between 1.6–11.2 nm h^{-1} (4.7 ± 2.6 nm h^{-1}), within the range reported from many other locations (Kulmala et al. 2004a; Kanawade et al. 2012).

4.2. Growth of Newly Formed Particles to CCN-Active Sizes

$N_{100-500}$, a surrogate of CCN-active size particles, was lower on sub-5 nm particle formation event days than non-event days (Figure 1). During non-event days, $N_{100-500}$ raised from the background level ($\sim$1500 cm^{-3}) to $\sim$1900 cm^{-3} in the morning, while N_{sub-5} remained constant at the background level of $\sim$1000 cm^{-3} during the whole day (Figure 1a). These elevated 100–500 nm particle concentrations (and hence high CS) were thus likely to suppress the occurrence of NPF. On event days, the $N_{100-500}$ remained relatively constant (Figure 1b). The lowest $N_{100-500}$ of $\sim$800 cm^{-3} was observed at the noontime, when there were high concentrations of new particles (N_{sub-5} and N_{5-25}). Afterwards, there was a slow increase of $N_{100-500}$ from 800 cm^{-3} to 1050 cm^{-3} throughout the night. This slow increase of $N_{100-500}$ reflects the CCN production, due to the growth of new particles.

Figure 2 shows the change in $N_{100-500}$ during a typical regional event, which lasted for five consecutive days (22–26 September 2012). After the very first NPF event on 22 September, $N_{100-500}$ increased slowly from $\sim$160 cm^{-3} around 14:00 PM up to $\sim$600 cm^{-3} around 1:00 AM in the next morning, while nucleation mode particles grew to $\sim$60 nm at the same time. In the morning of 23 September, a further growth was interrupted, perhaps due to the vertical dilution of surface air driven by the high incoming solar radiation in the clear sky in northwesterly air masses. As a result, $N_{100-500}$ decreased down to 280 cm^{-3} at 10:00 AM, which triggered another NPF event. This same cycle repeated for the forthcoming three days until the wind direction switched to the south on 24 September. Afterwards, new particles grew continuously to the accumulation mode in southerly air parcels, and as a result, $N_{100-500}$ increased steadily from 760 cm^{-3} to $\sim$2000 cm^{-3}.

Regional NPF events, consisting of 2 to 8 consecutive NPF event cycles, were common throughout the campaign period.

TABLE 3

Nucleation rate (J_1), formation rate of 5 nm particles (J_5), growth rate (GR), and survival ratios of 1–5 nm cluster-mode particles to 5–25 nm nucleation mode particles ($\Delta N_{5-25}/\Delta N_{1-5}$) and to 100–500 nm CCN ($\Delta N_{100-500}/\Delta N_{sub-5}$), for 18 Class-I NPF events observed during August–October 2012. SD = standard deviation

	Date	GR (nm h^{-1})	J_1 (cm^{-3} s^{-1})	J_5 (cm^{-3} s^{-1})	$\Delta N_{5-25}/\Delta N_{sub-5}$ (%)	$\Delta N_{100-500}/\Delta N_{sub-5}$ (%)
Non-events		—	0.1 ± 0.3	$(5.0 \pm 7.2) \times 10^{-3}$	—	—
Class -I Events	1 August	5.8	3.8	0.4	32.1	9.4
	6 August	3.2	2.5	0.3	26.4	9.0
	8 August	1.6	8.7	0.6	36.1	1.8
	17 August	8.8	9	1.5	25.4	1.7
	18 August	5	17.7	1.8	30.5	4.1
	9 September	3.2	2.8	0.4	23.1	6.3
	10 September	11.2	30.6	4.5	28.7	3.1
	14 September	5.9	3.2	0.5	32.4	7.8
	15 September	7.7	3.6	0.3	20.2	9.3
	22 September	6.6	42.6	2.9	18.0	0.4
	23 September	3.9	13.8	1.3	14.5	0.5
	24 September	2.7	12.4	0.5	9.7	2.1
	28 September	3.6	7.3	0.6	38.5	—
	1 October	4.9	5.2	0.4	18.0	1.7
	2 October	2.5	10.3	0.2	11.5	1.8
	10 October	2.5	0.8	0.1	18.0	6.2
	12 October	2.5	8.7	0.5	10.6	3.3
	15 October	2.3	15.3	1.4	21.9	—
	Mean $\pm$ SD	4.7 ± 2.6	11.0 ± 10.6	1.0 ± 1.1	23.1 ± 8.8	4.3 ± 3.2

This was perhaps due to relatively homogeneous meteorological conditions in large-scale air masses on those consecutive days. Such consecutive cycles of NPF events led to the enhancement of CCN. The enhancement factor (*EF*) of CCN within a regional NPF event was defined as the ratio of the highest $N_{100-500}$ measured at the end of the regional NPF event to the lowest $N_{100-500}$ at the beginning of the same regional NPF event. For example, the *EF* was 5.9 for the case shown in Figure 2. The *EF* of CCN in 13 regional NPF events observed between May and October ranged from 3.0 to 10.5 with an average of 4.7 (Table 4). This was roughly in similar *EF* ranges reported from urban, suburban, and pristine sites previously (Lihavainen et al. 2003; Kerminen et al. 2005; Laaksonen et al. 2005; Kuwata and Kondo 2008; Kuang et al. 2009; Wiedensohler et al. 2009; Asmi et al. 2011; Sihto et al. 2011; Yue et al. 2011; Kerminen et al. 2012; Wang et al. 2013). This indicates that regional NPF can enhance the CCN production also in forest regions.

The *GR* was highest in the BVOCs-rich southerly air masses and these high *GR* contributed to the enhanced production of CCN. The enhancement of CCN by available organic vapors was also indicated by a positive correlation between $N_{100-500}$ and isoprene (Figure 3a). This result implies that oxidation products of isoprene were likely involved in the growth of new particles. A positive correlation between $N_{100-500}$ and O_3 was also observed (Figure 3b). On the other hand, a positive correlation between $N_{100-500}$ and SO_2 was not observed. This indicates that CCN-active particles ($N_{100-500}$) at the Ozarks site were mainly associated with BVOCs-rich air masses, but not with sulfur plumes. This result is consistent with another observation which also showed that the CCN enhancement was more significant in a sulfur-poor atmosphere, where organic species facilitated the growth of new particles to CCN-active sizes (Yue et al. 2011). Our correlation analysis with BVOCs and ozone suggests that BOVCs oxidation products may have contributed to the CCN-active particle formation in this forest region, but further research is required to identify the chemical species and mechanisms involved in this process.

We used the survival rate to evaluate the contribution of NPF to CCN within an individual NPF event. For a typical Class-I NPF event occurring in relatively clean atmospheric conditions, one can assume that (i) pre-existing 100–500 nm particle concentrations remain nearly constant during the NPF event, and (ii) the CCN production from condensation or coagulation of pre-existing particles is negligible. Under these assumptions, the survival rate at which cluster mode particles grow to CCN during a NPF event was defined as the ratio of an increase in $N_{100-500}$ before and after the NPF event ($\Delta N_{100-500}$) versus an increase in sub-5 nm particles during the same NPF event (ΔN_{sub-5}). Similarly, the survival rate of 1–5 nm particles to 5–25 nm nucleation-mode particles was defined as
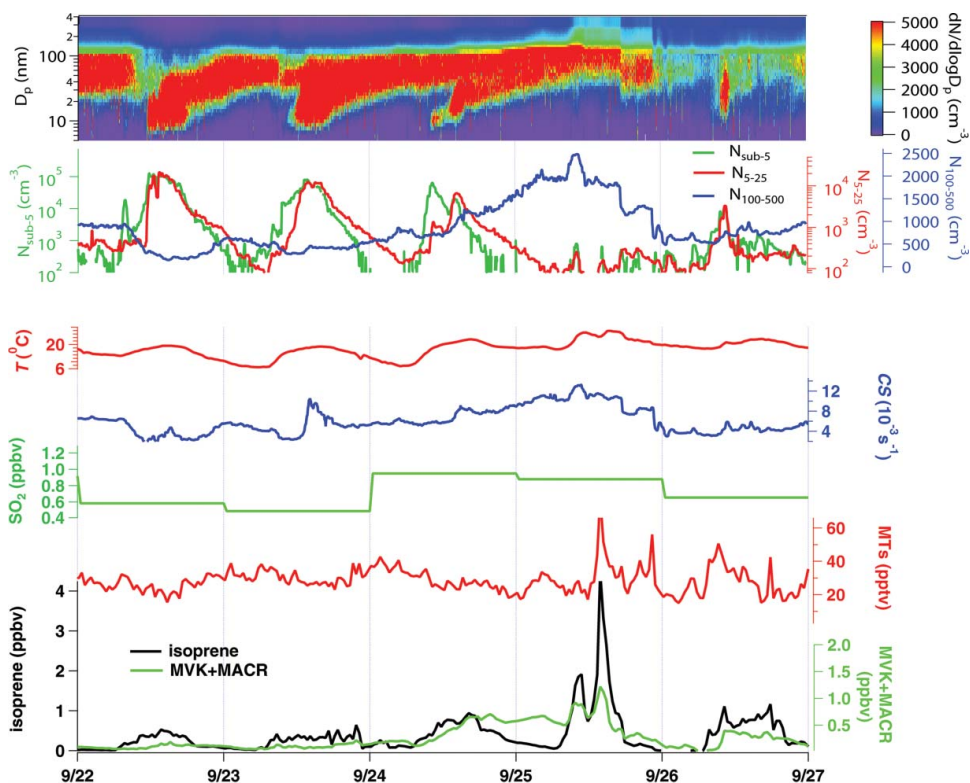
FIG. 2. The measured particle number size distribution, N_{sub-5}, N_{5-25}, $N_{100-500}$, ambient temperature, condensation sink (CS), SO$_2$, temperature (T), monoterpenes, isoprene, and MVK+MACR at Ozark, Missouri during 22–26 September 2012, where a typical regional NPF event was observed.

$\Delta N_{5-25}/\Delta N_{sub-5}$. During NPF events, 10–32% of 1–5 nm particles grew to 5–25 nm via particle coagulation (Table 3). Survival rates of 1–5 nm particles to CCN-active sizes ranged from 0.4–9%. Our estimations are within the same range of CCN production probabilities ($n_{100}/n_3 = 1$–20%) reported

from elsewhere, such as Boulder, Colorado; Atlanta, Georgia; and Tecamac, Mexico (Kuang et al. 2009). However, it should be noted that EFs and survival rates obtained in our study as well as in the cited studies (Lihavainen et al. 2003; Kuang et al. 2009; Wiedensohler et al. 2009; Yue et al. 2011; Wang

TABLE 4

Enhancement factors (EF) of CCN ($N_{100-500}$) resulted from regional NPF events. EF is defined as the ratio of $N_{100-500}$ at the beginning to the end of a regional NPF event

| Duration	$N_{100-500}$ at the start of an event (cm^{-3})	$N_{100-500}$ at the end of an event (cm^{-3})	EF
16–19 May	1035	3105	3.0
21–24 May	505	3151	6.2
2–4 June	866	1977	2.3
12–15 June	700	3145	4.5
22–24 June	724	3176	4.4
27–30 July	1093	3049	2.8
5–8 August	508	2186	4.3
16–25 August	267	2795	10.5
8–13 September	402	2621	6.5
14–16 September	535	2411	4.5
20–25 September	329	1952	5.9
1–3 October	1007	2455	2.4
6–9 October	327	1388	4.2
Mean $\pm$ SD	638 $\pm$ 288	2570 $\pm$ 572	4.7 $\pm$ 2.2
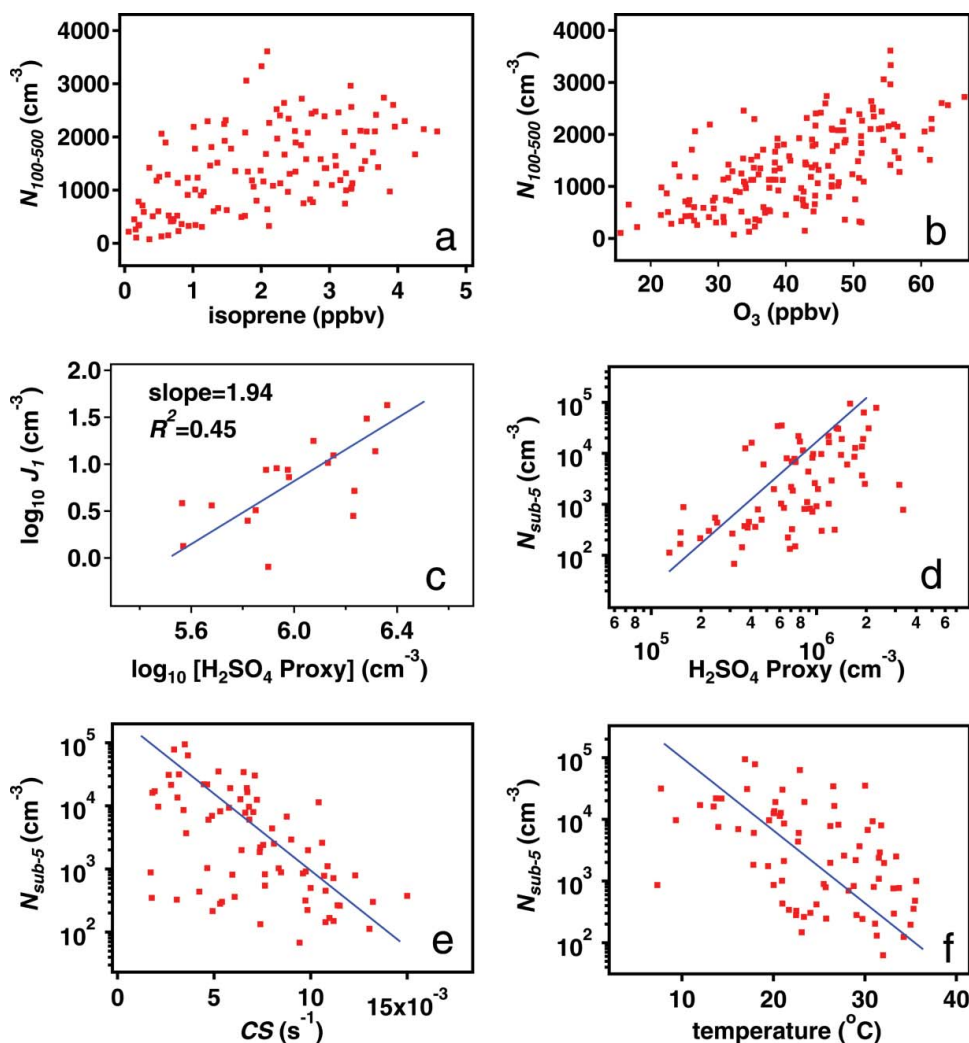
FIG. 3. Scatter plot of daily mean values of $N_{100-500}$ and isoprene (a), $N_{100-500}$ and O_3 (b) from 4 May–20 October 2012; Log J_1 vs. Log [H_2SO_4 Proxy] for 18 Class I NPF events (c), daily mean values of N_{sub-5} vs. H_2SO_4 Proxy (d), N_{sub-5} vs. CS (e), and N_{sub-5} vs. temperature (f) from 1 August–18 October 2012 at the Northern Ozarks site. Lines on (c), (d), (e), and (f) are drawn to guide the eye.

et al. 2013) did not take into account the change of CCN concentrations resulting from varying boundary layer heights or air mass dilutions before and after a NPF event. These effects were instead considered to be relatively minor. However, in the real atmosphere, it is possible that new particles were generated from a NPF event, and then transported to higher altitudes due to convection, dilution or air mixing. These new particles, while still growing large enough to become CCN, were not monitored by instruments located at the ground level or a fixed altitude. In this case, the CCN production may be underestimated.

4.3. Statistical Analysis for Different Air Masses

We examined the effects of potential precursor vapors and meteorological parameters on NPF in four types of air masses (Figure 4). A semi-empirical proxy for H_2SO_4 concentration was calculated from $k_{H2SO4} \times [SO_2] \times UV/CS$, where k_{H2SO4} is $8.4 \times 10^{-7} \times UV^{-0.68}$ m^2 W^{-1}s^{-1} (Petäjä et al. 2009; Yli-Juuti et al. 2011). The highest J_1, J_5, N_{sub-5}, and N_{5-25} were found in the northwesterly air masses, where SO_2 mixing ratios were lowest. The threshold SO_2 mixing ratio for sub-5 nm particles and NPF events was 0.1 ppbv and 0.24 ppbv, respectively. On several non-event days, SO_2 mixing ratios were actually higher than 0.24 ppbv. On the other hand, H_2SO_4 proxy and UV increased with increasing J_1, N_{sub-5}, N_{5-25} (Figure 4); both J_1 and N_{1-5} loosely correlated with H_2SO_4 proxy (Figure 3c and d). These results imply that while SO_2 was in general sufficient for NPF in the Ozark forest, H_2SO_4 and UV were limiting the NPF occurrence. However, relatively weak correlations between H_2SO_4 and J_1 ($R^2 = 0.45$) also suggest that nucleation rates were controlled by other chemical species as well.
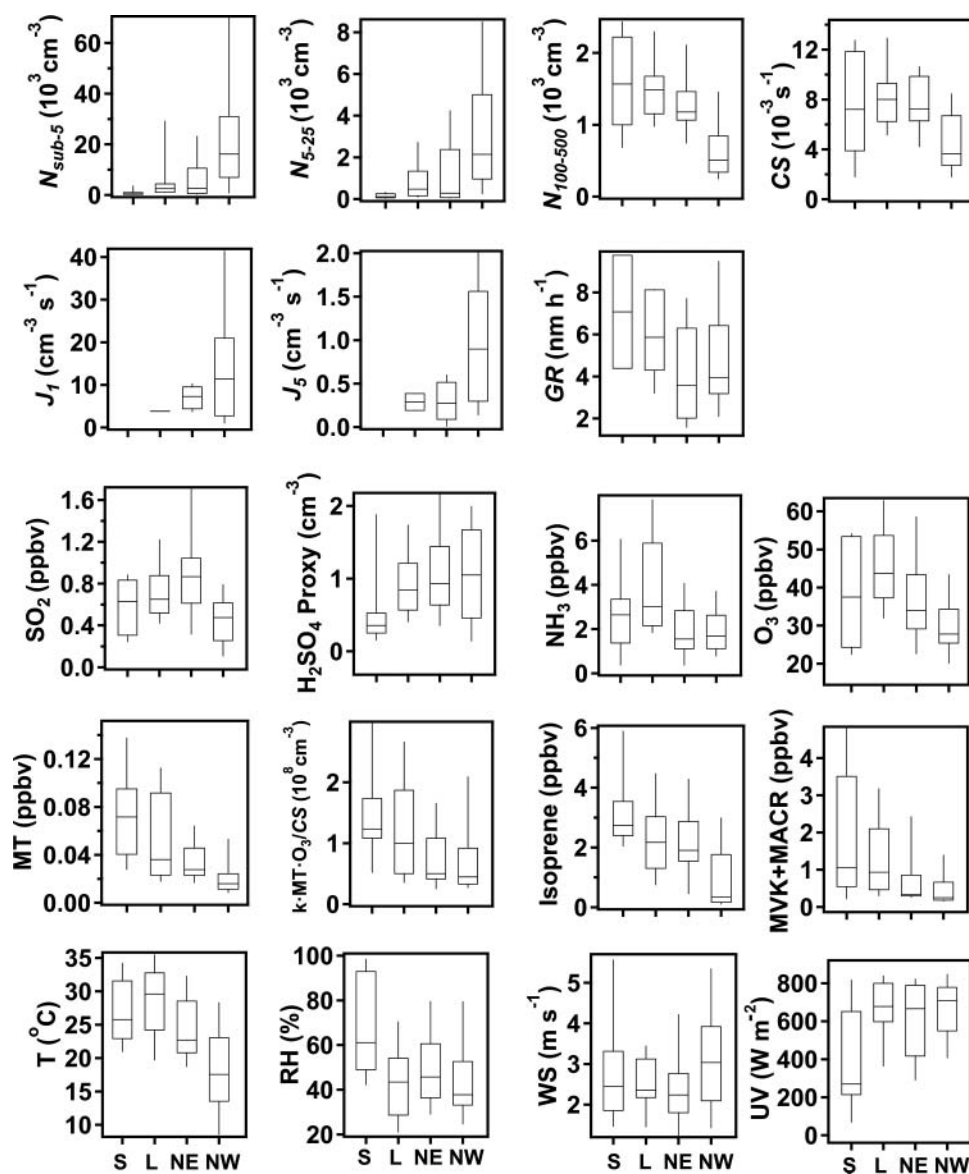
FIG. 4. Chemical species and meteorological parameters in four types of air masses at the Northern Ozarks site during total 61 typical observation days from 1 August–18 October 2012. The median (horizontal solid lines), the 75th and 25th percentile (boxes), the 90th and 10th percentile (solid whiskers) of daily mean values are shown. Daily mean values for the period between 9:00–15:00 LT, which was the strong sub-5 nm particle event period, was calculated for H_2SO_4 proxy, N_{sub-5}, N_{5-25}, $N_{100-500}$, CS, MT, isoprene, MVK+MACR, RH, Temperature, UV, and wind speed.

The MOZART model-predicted NH_3 mixing ratios ranged from 0.2 ppbv to 8 ppbv. The threshold NH_3 mixing ratio for the observed Class-I NPF was 0.44 ppbv in northwesterly air masses. Frequent NPF took place in NH_3-poor northwesterly (median 1.68 ppbv) and northeasterly (1.55 ppbv) air masses, while NPF was rare in both NH_3-rich southerly (2.64 ppbv) and local (3.0 ppbv) air masses.

Isoprene and MT mixing ratios ranged from 0.1–5.9 ppbv and 0.008–0.14 ppbv, respectively. The threshold isoprene and MT mixing ratios for NPF was 0.26 ppbv and 0.01 ppbv in northwesterly air masses. In southerly and local air masses where NPF was rarely observed, isoprene and MT mixing ratios were usually higher than 1 ppbv and 0.02 ppbv, respectively. Moreover, isoprene, MTs, and their first generation oxidation products (MVK+MACR and the $k \times MT \times O_3/CS$ product) were in the reverse order of J, N_{sub-5}, and N_{5-25}. Here, k is ozonolysis rate coefficient of α-pinene, which is the most abundant MT in the atmosphere (Guenther et al. 2012). As shown in Figure 2, the absence of NPF on 25 September was accompanied by the accumulation of isoprene, MTs, and MVK+MACR. There was also not a clear positive or negative correlation for N_{sub-5} and J_1 with norpinic acid or pinonaldehyde measured with PTR-TOF-MS, both of which are first-generation oxidation products of MT with ozone or hydroxyl radicals.
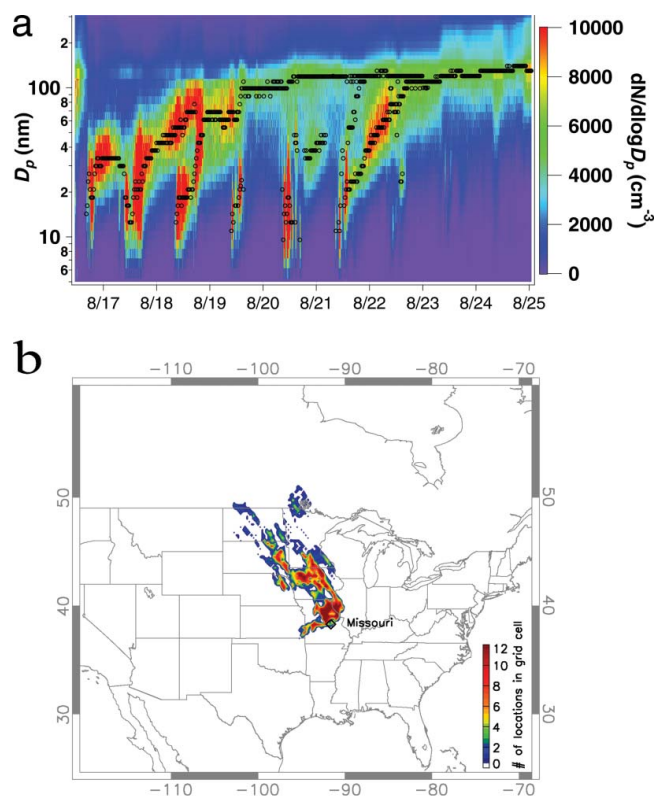
FIG. 5. (a) A regional NPF event that had a long time span of 9 days from 16–24 August 2012 at the Northern Ozarks site. The open circles on the particle number size distribution spectrum represent the particle mode diameter for each 5 min's size distribution. (b) The minimum spatial scale of the regional NPF event estimated for the same period is shown in colored areas.

CS in four air masses was negatively correlated with J, N_{sub-5}, and N_{5-25} (Figures 3e and 4). CS was $\sim 3.6 \times 10^{-3}$ s^{-1} in northwesterly air masses and $\sim 7.2 \times 10^{-3}$ s^{-1} in southerly air masses. Thus, it is likely that high CS suppressed the NPF occurrence. In addition to high CS, high temperatures (median 26 and 29°C) were another unfavorable condition for NPF in southerly and local air masses (Figures 3f and 4). These results imply that BVOCs-rich air parcels were favorable for the particle growth and the conversion of new particles to CCN active sizes, while higher aerosol loadings (and hence CS) and high temperatures in the same air masses inhibited the occurrence of NPF.

4.4. Spatial Scales of Regional NPF Events

The spatial scale of an NPF event indicates the extent to which NPF contributes to the aerosol loading at the regional scale. Two approaches have been typically applied in the literature to determine spatial scales of NPF. The first approach is based on simultaneous measurements at multiple stationary stations (Stanier et al. 2004; Dal Maso et al. 2007; Wehner et al. 2007; Crumeyrolle et al. 2010; Jeong et al. 2010), and another is based on the history of air mass back-trajectories (Vana et al. 2004; Hussein et al. 2009; Crippa and Pryor 2013). Here, we adopted the second approach.

Amongst 13 regional NPF events observed during the campaign, we chose a regional NPF event which took place on August 16–24 to examine the spatial scale of NPF (Figure 5a). The NPF first appeared at the noontime on 16 August. On the following 6 days, a group of new nucleation-mode particles formed every day and then merged with the Aitken mode particles formed on the previous day, and they eventually grew to ~ 150 nm. Assuming that the air parcel was homogeneous with respect to the characteristics of aerosols, we followed the back-trajectories for each time step (1 h) during the time span of this regional event and traced them back to the upwind locations where nucleation occurred. Once all these locations were plotted on the map, we estimated the minimum spatial scale of this regional NPF event. The minimum distance of this NPF event was ~ 1500 km, to the northwest of the Northern Ozarks site (Figure 5b). Since these locations only represent the upwind spatial scale of this regional NPF event, the actual spatial extent of the event could be even larger, if we include the region downwind of the measurement site. These results imply that NPF event in the Northern Ozarks site is a synoptic phenomenon that can affect aerosol loading in a spatial scale of at least 1500 km. Our estimated spatial scales are comparable to those reported from other studies in the northern Europe and the eastern North America (Vana et al. 2004; Hussein et al. 2009; Crippa and Pryor 2013).

5. CONCLUSIONS

We have conducted a field study over an Ozark forest dominated by isoprene emissions, from May to October, 2012. This forest site typically underwent four different types of air masses: the southerly BVOCs-rich, the northwesterly clean, the northeasterly SO_2-rich, and the slow moving local air masses. There was a significant suppression of sub-5 nm particles and NPF in southerly air masses with high abundance of BVOCs, and this was due to relatively low H_2SO_4 production, high CS, and high temperatures. The abundant BVOCs in the southerly air masses were, on the other hand, favorable for the particle growth to CCN active sizes. The sub-5 particle number concentrations ranged from the background level 1000 cm^{-3} up to $\sim 20,000$ cm^{-3} during the noontime event periods. Rather high J_1 (11.0 ± 10.6 cm^{-3} s^{-1}) were observed, one order of magnitude higher than J_5, indicating that most 1 nm clusters underwent coagulation losses, instead of growing from 1 nm to 5 nm. Within an individual NPF event, 9.7–32.1% of 1–5 nm particles grew to 5–25 nm particles and 0.4–9.4% of new particles grew to CCN-active sizes. NPF also took place continuously for several consecutive days at this forest site, indicative of a large regional scale of NPF over several hundred kilometers. During these regional NPF events, the production of CCN was enhanced, on average, by a factor of 4.7, indicating that Ozark forests can be important source of NPF and CCN production at the regional scale.

REFERENCES

Asmi, E., Kivekäs, N., Kerminen, V. M., Komppula, M., Hyvärinen, A. P., Hatakka, J., et al. (2011). Secondary New Particle Formation in Northern Finland Pallas Site Between the Years 2000 and 2010. *Atmos. Chem. Phys.*, 11(24):12959–12972.

Bonn, B., Boy, M., Kulmala, M., Groth, A., Trawny, K., Borchert, S., et al. (2009). A New Parametrization for Ambient Particle Formation over Coniferous Forests and its Potential Implications for the Future. *Atmos. Chem. Phys.*, 9(20):8079–8090.

Bonn, B., Hirsikko, A., Hakola, H., Kurten, T., Laakso, L., Boy, M., et al. (2007). Ambient Sesquiterpene Concentration and its Link to Air Ion Measurements. *Atmos. Chem. Phys.*, 7:2893–2916.

Bonn, B., Kulmala, M., Riipinen, I., Sihto, S.-L., and Ruuskanen, T. M. (2008). How Biogenic Terpenes Govern the Correlation Between Sulfuric Acid Concentrations and New Particle Formation. *J. Geophys. Res.*, 113 (D12):D12209.

Bonn, B., and Moortgat, G. K. (2002). New Particle Formation During a- and b-pinene Oxidation by O3, OH and NO3, and the Influence of Water Vapour: Particle Size Distribution Studies. *Atmos. Chem. Phys.*, 2: 183–196.

Bonn, B., and Moortgat, G. K. (2003). Sesquiterpene Ozonolysis: Origin of Atmospheric New Particle Formation from Biogenic Hydrocarbons. *Geophys. Res. Lett.*, 30(11):1585.

Crippa, P., and Pryor, S. C. (2013). Spatial and Temporal Scales of New Particle Formation Events in Eastern North America. *Atmos. Environ.*, 75 (0):257–264.

Crumeyrolle, S., Manninen, H. E., Sellegri, K., Roberts, G., Gomes, L., Kulmala, M., et al. (2010). New Particle Formation Events Measured on Board the ATR-42 Aircraft during the EUCAARI Campaign. *Atmos. Chem. Phys.*, 10(14):6721–6735.

Dal Maso, M., Kulmala, M., Riipinen, I., Wagner, R., Hussein, T., Aalto, P., et al. (2005). Formation and Growth Rates of Fresh Atmospheric Aerosols: Eight Years of Aerosol Size Distribution Data from SMEARII, Hyytiälä, Finland. *Boreal Environ. Res.*, 10:323–336.

Dal Maso, M., Sogacheva, L., Aalto, P. P., Riipinen, I., Komppula, M., Tunved, P., et al. (2007). Aerosol Size Distribution Measurements at Four Nordic Field Stations: Identification, Analysis and Trajectory Analysis of New Particle Formation Bursts. *Tellus B*, 59(3):350–361.

Draxler, R. R., and Rolph, G. D. (2003). HYSPLIT (Hybrid Single-Particle Langrangian Integrated Trajectory) Model Access Edited, NOAA Air Resources Laboratory.

Ehn, M., Junninen, H., Petaja, T., Kurten, T., Kerminen, V. M., Schobesberger, S., et al. (2010). Composition and Temporal Behavior of Ambient Ions in the Boreal Forest. *Atmos. Chem. Phys.*, 10(17):8513–8530.

Ehn, M., Thornton, J. A., Kleist, E., Sipila, M., Junninen, H., Pullinen, I., et al. (2014). A Large Source of Low-Volatility Secondary Organic Aerosol. *Nature*, 506(7489):476–479.

Emmons, L. K., Walters, S., Hess, P. G., Lamarque, J. F., Pfister, G. G., Fillmore, D., et al. (2010). Description and Evaluation of the Model for Ozone and Related Chemical Tracers, version 4 (MOZART-4). *Geosci. Model Dev.*, 3(1):43–67.

Greenberg, J. P., Guenther, A., Petron, G., Wiedinmyer, C., Vega, O., Gatti, L. V., et al. (2004). Biogenic VOC Emissions from Forested Amazonian Landscapes. *Global Biogeochem. Cycles*, 10:651–662.

Guenther, A. B., Jiang, X., Heald, C. L., Sakulyanontvittaya, T., Duhl, T., Emmons, L. K., et al. (2012). The Model of Emissions of Gases and Aerosols from Nature version 2.1 (MEGAN2.1): An Extended and Updated Framework for Modeling Biogenic Emissions. *Geosci. Model Dev.*, 5 (6):1471–1492.

Guenther, A. B., Hewitt, C. N., Erickson, D., Fall, R., Geron, C., Graedel, T., et al. (1995). A Global Model of Natural Volatile Organic Compound Emissions. *J. Geophys. Res.*, 100:8873–8892.

Held, A., Nowak, A., Birmili, W., Wiedensohler, A., Forkel, R., and Klemm, O. (2004). Observations of Particle Formation and Growth in a Mountainous Forest Region in Central Europe. *J. Geophys. Res.*, 109:D23204.

Hussein, T., Junninen, H., Tunved, P., Kristensson, A., Dal Maso, M., Riipinen, I., et al. (2009). Time Span and Spatial Scale of Regional New Particle Formation Events over Finland and Southern Sweden. *Atmos. Chem. Phys.*, 9(14):4699–4716.

Jeong, C. H., Evans, G. J., McGuire, M. L., Chang, R. Y. W., Abbatt, J. P. D., Zeromskiene, K., et al. (2010). Particle Formation and Growth at Five Rural and Urban Sites. *Atmos. Chem. Phys.*, 10(16):7979–7995.

Kanawade, V., Benson, D. R., and Lee, S.-H. (2012). Statistical Analysis of 4 Year Measurements of Aerosol Sizes in a Semi-Rural U.S. Continental Environment. *Atmos. Environ.*, 59:30–38.

Kanawade, V. P., Guenther, A. B., Jobson, B. T., Erupe, M. E., Pressely, S. N., Tripathi, S. N., et al. (2011). Isoprene Suppression of New Particle Formation in a Mixed Decideous Forest. *Atmos. Chem. Phys.*, 11:6013–6027.

Kaser, L., Karl, T., Schnitzhofer, R., Graus, M., Herdlinger-Blatt, I. S., DiGangi, J. P., et al. (2013). Comparison of Different Real Time VOC Measurement Techniques in a Ponderosa Pine Forest. *Atmos. Chem. Phys.*, 13(5):2893–2906.

Kerminen, V.-M., Lihavainen, H., Komppula, M., and Viisanen, Y. (2005). Direct Observational Evidence Linking Atmospheric Aerosol Formation and Cloud Droplet Activation. *Geophys. Res. Lett.*, 32.

Kerminen, V. M., Paramonov, M., Anttila, T., Riipinen, I., Fountoukis, C., Korhonen, H., et al. (2012). Cloud Condensation Nuclei Production Associated with Atmospheric Nucleation: A Synthesis Based on Existing Literature and New Results. *Atmos. Chem. Phys.*, 12 (24):12037–12059.

Kiendler-Scharr, A., Wildt, J., Dal Maso, M., Hohaus, T., Kleist, E., Mente, T. F., et al. (2009). New Particle Formation in Forests Inhibited by Isoprene Emissions. *Nature*, 461:381–384.

Kiendler-Scharr, A., Andres, S., Bachner, M., Behnke, K., Broch, S., Hofzumahaus, A., et al. (2012). Isoprene in Poplar Emissions: Effects on New Particle Formation and OH Concentrations. *Atmos. Chem. Phys.*, 12 (2):1021–1030.

Kuang, C., McMurry, P. H., and McCormick, A. V. (2009). Determination of Cloud Condensation Nuclei Production from Measured New Particle Formation Events. *Geophys. Res. Lett.*, 36(9):L09822.

Kuang, C., McMurry, P. H., McCormick, A. V., and Eisele, F. (2008). Dependence of Nucleation Rates on Sulfuric Acid Vapor Concentration in Diverse Atmospheric Locations. *J. Geophys. Res.*, 133(D10209).

Kulmala, M., dal Maso, M., Makela, J. M., Pirjola, L., Vakeva, M., Aalto, P., et al. (2001). On the Formation, Growth, and Composition of Nucleation Mode Particles. *Tellus*, 53B:479–490.

Kulmala, M., Laakso, L., Lehtinen, K. E. J., Riipinen, I., Dal Maso, M., Lauria, A., et al. (2004b). Formation and Growth Rates of Ultrafine Atmosphere Particles: A Review of Observations. *J. Aerosol., Sci.*, 35:143–176.

Kulmala, M., Vehkamaki, H., Petaja, T., dal Maso, M., Lauri, A., Kerminen, V. M., et al. (2004a). Formation and Growth Rates of Ultrafine Atmospheric Particles: A Review of Observations. *J. Aerosol Sci.*, 35(2):143–176.

Kulmala, M., Kontkanen, J., Junninen, H., Lehtipalo, K., Manninen, H. E., Nieminen, T., et al. (2013). Direct Observations of Atmospheric Aerosol Nucleation. *Science*, 339(6122):943–946.

Kuwata, M., and Kondo, Y. (2008). Dependence of Size-Resolved CCN Spectra on the Mixing State of Nonvolatile Cores Observed in Tokyo. *J. Geophys. Res.: Atmospheres*, 113(D19):D19202.

Laakso, L., Laakso, H., Aalto, P. P., Keronen, P., Petäjä, T., Nieminen, T., et al. (2008). Basic Characteristics of Atmospheric Particles, Trace Gases and Meteorology in a Relatively Clean Southern African Savannah Environment. *Atmos. Chem. Phys.*, 8:4823–4839.

Laaksonen, A., Hamed, A., Joutsensaari, J., Hiltunen, L., Cavalli, F., Junkermann, W., et al. (2005). Cloud Condensation Nucleus Production from Nucleation Events at a Highly Polluted Region. *Geophys. Res. Lett.*, 32 (6):L06812.

Lehtipalo, K., Sipila, M., Junninen, H., Ehn, M., Berndt, T., Kajos, M. K., et al. (2011). Observations of Nano-CN in the Nocturnal Boreal Forest. *Aerosol Sci. Technol.*, 45(4):499–509.

Lihavainen, H., Kerminen, V. M., Komppula, M., Hatakka, J., Aaltonen, V., Kulmala, M., et al. (2003). Production of "potential" Cloud Condensation Nuclei Associated with Atmospheric New-Particle Formation in Northern Finland. *J. Geophys. Res.*, 108(D24):4782.

Lin, Y.-H., Zhang, H., Pye, H. O. T., Zhang, Z., Marth, W. J., Park, S., et al. (2013). Epoxide as a Precursor to Secondary Aerosol Formation from Isoprene Photooxidation in the Presence of Nitrogen Oxides. *Proc. Natl. Acad. Sci.*, 110(17):6718–23.

Mäkelä, J. M., Alto, P., Jokinen, V., Pohja, T., Nissenin, A., Palmroth, S., et al. (1997). Observations of Ultrafine Aerosol Particle Formation and Growth in Boreal Forest. *Geophys. Res. Lett.*, 24:1219–1222.

Matsui, H., Koike, M., Takegawa, N., Kondo, Y., Takami, A., Takamura, T., et al. (2013). Spatial and Temporal Variations of New Particle Formation in East Asia using an NPF-explicit WRF-chem Model: North-South Contrast in New Particle Formation Frequency. *J. Geophys. Res.*, 118 (20):11647–11663.

Ortega, I. K., Suni, T., Boy, M., Grönholm, T., Manninen, H. E., Nieminen, T., et al. (2012). New Insights into Nocturnal Nucleation. *Atmos. Chem. Phys.*, 12(9):4297–4312.

Petäjä, T., Mauldin III, R. L., Kosciuch, E., McGrath, J., Nieminen, T., Paasonen, P., et al. (2009). Sulfuric Acid on OH Concentrations in Boreal Forest Site. *Atmos. Chem. Phys.*, 9:7435–7448.

Pierce, J. R., and Adams, P. J. (2009). Uncertainty in Global CCN Concentrations from Uncertain Aerosol Nucleation and Primary Emission Rates. *Atmos. Chem. Phys.*, 9(4):1339–1356.

Pöhlker, C., Wiedemann, K. T., Sinha, B., Shiraiwa, M., Gunthe, S. S., Smith, M., et al. (2012). Biogenic Potassium Salt Particles as Seeds for Secondary Organic Aerosol in the Amazon. *Science*, 337(6098):1075–1078.

Poschl, U., Martin, S. T., Sinha, B., Chen, Q., Gunthe, S. S., Huffman, J. A., et al. (2010). Rainforest Aerosols as Biogenic Nuclei of Clouds and Precipitation in the Amazon. *Science*, 329(5998):1513–1516.

Potosnak, M. J., LeStourgeon, L., Pallardy, S. G., Hosman, K. P., Gu, L., Karl, T., et al. (2014). Observed and Modeled Ecosystem Isoprene Fluxes from an Oak-Dominated Temperate Forest and the Influence of Drought Stress. *Atmos. Environ.*, 84(0):314–322.

Riccobono, F., Rondo, L., Sipilä, M., Barmet, P., Curtius, J., Dommen, J., et al. (2012). Contribution of Sulfuric Acid and Oxidized Organic Compounds to Particle Formation and Growth. *Atmos. Chem. Phys.*, 12:9427–9439.

Schobesberger, S., Junninen, H., Bianchi, F., Lönn, G., Ehn, M., Lehtipalo, K., et al. (2013). Molecular Understanding of Atmospheric Particle Formation from Sulfuric Acid and Large Oxidized Organic Molecules. *Proc. Natl. Acad. Sci.*, 110:17223–17228.

Seinfeld, J. H., and Pandis, S. N. (2006). *Atmos. Chem. Phys.: From Air Pollution to Climate Change*. 2nd ed., John Wiley and Sons. Inc., New York.

Sihto, S.-L., Kulmala, M., Kerminen, V. M., Dal Maso, M., Petäjä, T., Riipinen, I., et al. (2006). Atmospheric Sulfuric Acid and Aerosol Formation: Implications form Atmospheric Measurements for Nucleation and Early Growth Mechanisms. *Atmos. Chem. Phys.*, 6:4079–4091.

Sihto, S. L., Mikkilä, J., Vanhanen, J., Ehn, M., Liao, L., Lehtipalo, K., et al. (2011). Seasonal Variation of CCN Concentrations and Aerosol Activation Properties in Boreal Forest. *Atmos. Chem. Phys.*, 11(24):13269–13285.

Spirig, C., Guenther, A., Greenberg, J. P., Calanca, P., and Tarvainen, V. (2004). Tethered Balloon Measurements of Biogenic Volatile Organic Compounds at a Boreal Forest Site. *Atmos. Chem. Phys.*, 4:215–229.

Spracklen, D. V., Carslaw, K. S., Kulmala, M., Kerminen, V. M., Sihto, S. L., Riipinen, I., et al. (2008). Contribution of Particle Formation to Global Cloud Condensation Nuclei Concentrations. *Geophys. Res. Lett.*, 35(6): L06808.

Stanier, C. O., Khlystov, A. Y., and Pandis, S. N. (2004). Ambient Aerosol Size Distributions and Number Concentrations Measured during the Pittsburgh Air Quality Study (PAQS). *Atmos. Environ.*, 38(20):3275–3284.

Surratt, J. D., Chan, A. W. H., Eddingsaas, H. E., Chan, M., Loza, C. L., Kwan, A. J., et al. (2010). Reactive Intermediates Revealed in Secondary Organic Aerosol Foramtion from Isoprene. *Proc. Natl. Acad. Sci.*, 107:6640–6645.

Vana, M., Kulmala, M., Dal Maso, M., Hõrrak, U., and Tamm, E. (2004). Comparative Study of Nucleation Mode Aerosol Particles and Intermediate Air Ions Formation Events at Three Sites. *J. Geophys. Res.*, 109(D17): D17201.

Vanhanen, J., Mikkila, J., Lehtipalo, K., Sipila, M., Manninen, H. E., Siivola, E., et al. (2011). Particle Size Magnifier for Nano-CN Detection. *Aerosol Sci. Technol.*, 45(4):533–542.

von der Weiden, S. L., Drewnick, F., and Borrmann, S. (2009). Particle Loss Calculator – a New Software Tool for the Assessment of the Performance of Aerosol Inlet Systems. *Atmos. Meas. Tech.*, 2(2):479–494.

Wang, Z. B., Hu, M., Sun, J. Y., Wu, Z. J., Yue, D. L., Shen, X. J., et al. (2013). Characteristics of Regional New Particle Formation in Urban and Regional Background Environments in the North China Plain. *Atmos. Chem. Phys.*, 13(8):12495–12506.

Wehner, B., Siebert, H., Stratmann, F., Tuch, T., Wiedensohler, A., PetaJa, T., et al. (2007). Horizontal Homogeneity and Vertical Extent of New Particle Formation Events. *Tellus B*, 59(3):362–371.

Wiedensohler, A., Cheng, Y. F., Nowak, A., Wehner, B., Achtert, P., Berghof, M., et al. (2009). Rapid Aerosol Particle Growth and Increase of Cloud Condensation Nucleus Activity by Secondary Aerosol Formation and Condensation: A Case Study for Regional Air Pollution in Northeastern China. *J. Geophys. Res.*, 114(D2):D00G08.

Wiedinmyer, C., Greenberg, J., Guenther, A., Hopkins, B., Baker, K., Geron, C., et al. (2005). Ozarks Isoprene Experiment (OZIE): Measurements and Modeling of the "isoprene volcano". *J. Geophys. Res.*, 110(D18):D18307.

Yli-Juuti, T., Nieminen, T., Hirsikko, A., Aalto, P. P., Asmi, E., Hõrrak, U., et al. (2011). Growth Rates of Nucleation Mode Particles in Hyytiälä During 2003–2009: Variation with Particle Size, Season, Data Analysis Method and Ambient Conditions. *Atmos. Chem. Phys.*, 11(24):12865–12886.

Yu, F., and Luo, G. (2009). Simulation of Particle Size Distribution with a Global Aerosol Model: Contribution of Nucleation to Aerosol and CCN Number Concentrations. *Atmos. Chem. Phys.*, 9(20):7691–7710.

Yu, H., Hallar, A. G., You, Y., Sedlacek, A., Springston, S., Kanawade, V. P., et al. (2014). Sub-3-nm Particles Observed at the Coastal and Continental Sites in the United States. *J. Geophys. Res.*, 119(2):2013JD020841.

Yue, D. L., Hu, M., Zhang, R. Y., Wu, Z. J., Su, H., Wang, Z. B., et al. (2011). Potential Contribution of New Particle Formation to Cloud Condensation Nuclei in Beijing. *Atmos. Environ.*, 45(33):6070–6077.

Zhang, R., Khalizov, A., Wang, L., Hu, M., and Xu, W. (2012). Nucleation and Growth of Nanoparticles in the Atmosphere. *Chem. Rev.*, 112(3):957–2011.

Zhang, R., Wang, L., Khalizov, A. F., Zhao, J., Zheng, J., McGraw, R. L., et al. (2009). Formation of Nanoparticles of Blue Haze Enhanced by Anthropogenic Pollution. *Proc. Natl. Acad. Sci.*, 106(42):17650–17654.

Zhao, J., Ortega, J., Chen, M., McMurry, P. H., and Smith, J. N. (2013). Dependence of Particle Nucleation and Growth on High-Molecular-Weight Gas-Phase Products During Ozonolysis of α-pinene. *Atmos. Chem. Phys.*, 13(15):7631–7644.